









Structural and electronic evidence of boron atomic chains

Yuki Tsujikawa ¹, Masafumi Horio ¹, Xiaoni Zhang,¹ Tomoaki Senoo,¹ Takeru Nakashima ², Yasunobu Ando ²,
Taisuke Ozaki,¹ Izumi Mochizuki,³ Ken Wada,³ Toshio Hyodo ³, Takushi Iimori,¹
Fumio Komori ¹, Takahiro Kondo ⁴ and Iwao Matsuda ^{5,*}

¹*Institute for Solid State Physics, The University of Tokyo, Kashiwa, Chiba 277-8581, Japan*

²*CD-FMat, National Institute of Advanced Industrial Science and Technology (AIST), Tsukuba, Ibaraki 305-8560, Japan*

³*Institute of Materials Structure Science, High Energy Accelerator Research Organization (KEK), Tsukuba, Ibaraki 305-0801, Japan*

⁴*Faculty of Pure and Applied Sciences, University of Tsukuba, Tsukuba, Ibaraki 305-8573, Japan*

⁵*Institute for Solid State Physics, The University of Tokyo, Kashiwa Chiba 277-8581, Japan*



(Received 7 June 2022; revised 3 October 2022; accepted 24 October 2022; published 8 November 2022)

The structure and chemical state of a boron chain, isoelectronic to polycumulene, were obtained with a combination of positron diffraction, photoelectron spectroscopy, and first-principles calculations. In the present work, an array of boron chains was found in a copper boride layer on a metal crystal substrate. The band structure of this material was determined to be electronically doped and hybridized by neighboring copper atoms. These boron atom chains exhibit a unique electrophilic character that is specific to the element. The properties of boron chains in the copper boride layer and the substrate effect are systematically investigated together.

DOI: [10.1103/PhysRevB.106.205406](https://doi.org/10.1103/PhysRevB.106.205406)

I. INTRODUCTION

Atomic chains represent useful systems for developing one-dimensional (1D) physics. Theoretically, an ideal 1D system can be considered a string comprising an infinite number of atoms that stand freely in space [1,2]. Experimentally, this is possible only in the case of a few atoms that are connected between atomically sharp probes or a periodic array of atomic chains prepared on the surface of a template. The ongoing development of surface-sensitive techniques has elucidated the structures and unique 1D states of atomic wires composed of various elements [3–8]. As an example, indium chains with a width of four atoms prepared on solid surfaces show a Peierls-type metal-insulator transition [3,4]. The addition of gold to a vicinal silicon surface has been found to result in the formation of silicon atom chains with a Z_3 charge density wave [6]. Cobalt chains at the step edges of a platinum surface are characterized by large localized orbital moments and correspondingly large magnetic anisotropy energies compared with two-dimensional (2D) and three-dimensional (3D) cobalt [8]. Recently, there have also been reports concerning low-dimensional boron-based materials, such as borophene [9–12] and 2D boride [13,14], and it has been proposed that boron chains with a single-atom width can form periodically on a copper crystal surface, as shown in Fig. 1(a) [15]. Since 2D boron materials have unique electronic structures [16–18], including Dirac fermions [16], it is expected that novel atomic chains comprising 1D boron could potentially be obtained with properties specific to the element. Thus, there is significant interest in determining the atomic arrangement and electronic states of this material.

In the present research, we conducted structural and chemical analyses of a boron layer on a Cu(111) substrate using the surface-sensitive techniques positron diffraction [19–23] and photoelectron spectroscopy. A copper boride (Cu boride) surface overlayer composed of a periodic array of boron atom chains with a zigzag structure was obtained. Systematic experiments indicated a direct relationship between the 1D atomic structure of this material and the negative charges on the boron atoms. First-principles calculations accurately reproduced the experimental spectroscopy data and showed that the boron atom chains can be isoelectronic to polycumulene, an unsaturated chain of carbon atoms. The electronic structure of the Cu boride layer examined in this work can be theoretically explained based on electronic doping and hybridization of the band structure of the boron wire by neighboring copper atoms. Systematic structural optimizations of the overlayer on a metal surface further unveiled that the boron chains protrude toward the substrate. The amount and the direction of the boron protrusion were found to sensitively depend on the layer height. The present results indicate characteristic features of low-dimensional boron that could be applied in the design of novel functional materials with uses in future devices.

II. EXPERIMENTAL AND CALCULATION METHODS

A sample was prepared on the surface of a commercial Cu(111) crystal (Surface Preparation Laboratory). The substrate was first cleaned by applying several cycles of Ar⁺ sputtering at 0.5 kV and annealing at 600 °C, after which the crystallinity of the material was confirmed by obtaining low-energy electron diffraction (LEED) and reflection high-energy electron diffraction (RHEED) patterns. Boron (99.999% pure) was subsequently deposited on the Cu(111) at 500 °C. The

*imatsuda@issp.u-tokyo.ac.jp

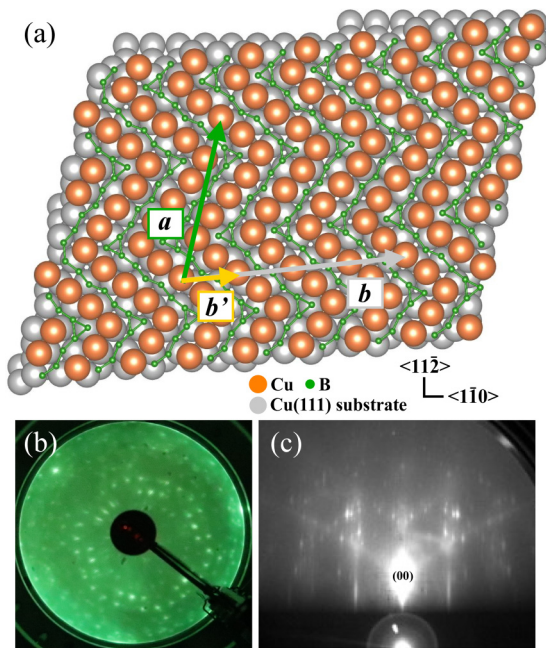


FIG. 1. The structure of the boron-based material on Cu(111) with measured diffraction patterns. (a) A structural model of the Cu boride layer on Cu(111). Vectors of the unit cell of the Cu boride $\sqrt{73} \times \sqrt{39}$ superstructure with Cu substrates are indicated by green and gray arrows (**a**, **b**), and the lattice vectors of only the overlayer Cu boride are marked by green and yellow arrows (**a'**, **b'**). The symmetric directions of the Cu(111) substrate are shown at the bottom right. (b) A LEED pattern acquired at an electron energy of 55 eV and (c) a RHEED pattern at 15 keV with the incident beam along the $\langle 1\bar{1}0 \rangle$ direction of the Cu substrate. The (00) spot is labeled.

formation of the surface specimen was checked by LEED and RHEED.

The structure of the sample surface was examined using total-reflection high-energy positron diffraction (TRHEPD), performed at the Slow Positron Facility at High Energy Accelerator Research Organization (KEK) [24]. The atomic arrangement was determined by acquiring rocking curves, which are the intensity profile of the specular (00)-spot beam with a glancing angle, combined with simulations based on a dynamical diffraction theory [25–27]. Details of the TRHEPD analysis process were provided in prior publications [19,28]. Chemical analysis was carried out using high-resolution x-ray photoelectron spectroscopy (XPS) performed on the BL07LSU soft x-ray beamline at the SPring-8 facility [29,30]. All data were obtained at room temperature.

To analyze the experimental results from the theoretical point of view, first-principles calculations are applied to evaluate electronic states (molecular orbitals and band structures), the XPS spectrum, and chemical potentials, employing the OpenMX (version 3.9.2) package [31,32]. OpenMX is a highly efficient first-principles calculation code combining an optimized pseudoatomic basis set and norm-conserving pseudopotentials [33]. Throughout the present work, the exchange-correlation functional was used with the generalized gradient approximation proposed by Perdew *et al.* [34]. Details of the individual calculations are as follows.

Molecular orbitals. The electronic calculation was made with a cutoff energy of 220 Ry and an optimization criterion of 1.0×10^{-4} Ry/bohr. The basis sets was B7.0-s3p2d2.

XPS simulation. The XPS spectrum was calculated based on the Janak theorem that applies to metallic systems [35–37]. The electron binding energies associated with the B sites were calculated with $1 \times 1 \times 1$ k points and a cutoff energy of 320 Ry. The basis sets for the reference ground state calculations were B7.0-s3p2d1 and Cu6.0H-s3p2d1, while the core hole state was treated using the penalty functional with the B7.0_1s_CH-s3p2d basis set.

Band calculation of a layer. Calculations of band dispersion curves were performed with $15 \times 10 \times 1$ k points and a cutoff energy of 250 Ry. The basis sets were B7.0-s3p2d and Cu6-s3p2d2f1.

Calculation of a layer/substrate system. Calculations of an overlayer on the substrate were made with $1 \times 1 \times 1$ k points, a cutoff energy of 400 Ry, and an optimization criterion of 3.0×10^{-5} Ry/bohr. The basis sets were B7.0-s2p2d1 and Cu6.0H-s3p2d1. To give the projected density of states (PDOS), the Gaussian broadening width was set at 0.1 eV. Chemical potentials with respect to the vacuum level were evaluated via the effective screening medium (ESM) method [38] that was implemented in OpenMX (version 3.9.2) [32]. The ESM calculation of a system was held under the boundary “vacuum/metal” condition of a neutral charge.

III. RESULTS AND DISCUSSION

By deposition of boron on a Cu(111) crystal surface, a 2D ordered phase was observed by LEED and RHEED, as given in Figs. 1(b) and 1(c), respectively. The diffraction patterns can be reproduced by a long-range order of the $\sqrt{73} \times \sqrt{39}$ superstructure on Cu(111) with the lattice vectors, illustrated in the atomic model in Fig. 1(a) as (**a**, **b**). The unit cell of the 2D phase has lattice parameters of $a = 15.99$ Å, $b = 21.87$ Å, and $\theta = 70.28^\circ$, where θ is the angle between vectors **a** and **b**. To understand the diffraction patterns, one must consider the contributions from the six domains that are equivalently grown in the two mirror-symmetric directions on the three-fold symmetric substrate of Cu(111). Patterns of LEED and RHEED for a single-domain $\sqrt{73} \times \sqrt{39}$ phase are given in Appendix A for reference. Comparisons between the simulation and the experiment show good agreement in Figs. 2(a) and 2(b) for LEED and Figs. 2(c) and 2(d) for RHEED. One can find one-to-one correspondence of the unique local patterns, labeled α , β , γ , and δ , between Figs. 2(a) and 2(b). In Figs. 2(c) and 2(d), the experimental RHEED spots overlap at the expected positions of the simulation. The results of the present diffraction analyses of electrons are consistent with previous research on the same ordered phase of the surface [12,15]. Based on the periodicity of the $\sqrt{73} \times \sqrt{39}$ superstructure, positions and properties of atoms in the unit cell are examined in the following analyses with positrons (TRHEPD) and with photoelectrons (XPS).

Figure 3(a) shows the TRHEPD rocking curves obtained from the surface boron material under the one-beam condition [26] to allow the analysis of atomic composition and height profiles. The experimental results are in better agreement with the simulated curve generated from a 2D Cu boride model

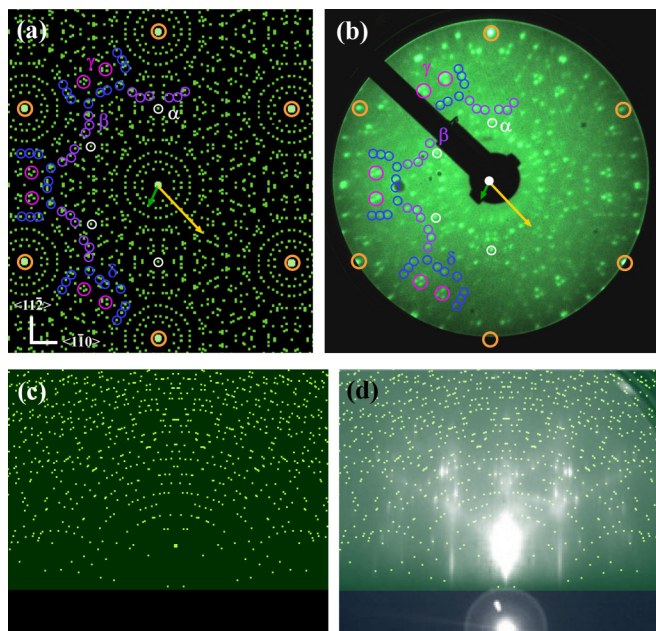


FIG. 2. Electron diffraction patterns of the $\sqrt{73} \times \sqrt{39}$ superstructure. (a) The reciprocal lattice of long-period $\sqrt{73} \times \sqrt{39}$ that corresponds to the expected LEED pattern. (b) The experimental LEED pattern taken at 81.5 eV. The characteristic spots are indicated by circles of different colors and labels (α , β , γ , and δ). Reciprocal vectors of the 2D ordered phase are illustrated by green and yellow arrows. The fundamental 1×1 spots of the Cu(111) substrate are also indicated by orange circles. (c) Expected locations of RHEED spots of the ordered phase. The pattern is simulated under the same beam condition as the experiment. (d) Overlap of the simulated and experimental RHEED patterns.

than with the curve of a borophene model [12,15]. The better matching with the model [Fig. 1(a)] was also confirmed for the TRHEPD results [Figs. 3(b) and 3(c)], obtained under the many-beam condition [27]. While the one-beam condition corresponds to an incident beam along an off-symmetric direction, the many-beam condition uses the beam along a symmetric direction. A combination of these measurement conditions allows us to experimentally determine the detailed atomic arrangement of the 2D Cu boride, including B-B lengths in the chain. It is of note that the structure model was taken from a previous report [15], and further TRHEPD analysis of the layer height found this structure to have an accuracy of $<0.1 \text{ \AA}$. These data provide evidence that the structure of the 2D boron-based material corresponds to that of 2D Cu boride, Cu_8B_{14} , with a periodic array of boron atom chains, as illustrated in Fig. 1(a). It is of note that experimental intensity appears to be low when compared with the simulation at a glancing angle $<2^\circ$. This is due to the ultrahigh surface sensitivity of the TRHEPD method, in which the highly oblique beam of positrons was blocked by microstructures on a surface, such as steps or remanent roughness from the sputtering process for surface cleaning. In the present research, the experimental limitation has a negligible influence on the surface structure analysis.

The chemical composition of 2D Cu boride was assessed by obtaining Cu $2p_{3/2}$ and B $1s$ core-level XPS data, as shown

in Fig. 4. While a pristine surface of Cu(111) is composed of a single chemical component of the Cu atom in addition to a negligible defect component, the 2D Cu boride sample has two Cu components of the surface layer (L) and in the bulk (Bu). These assignments were confirmed by spectral variations with the emission angle. The photoemission intensity of the layer component increased when the spectrum was obtained using surface-sensitive conditions (that is, with a large emission angle). The appearance of the peak related to the layer component at a higher binding energy than the bulk component indicates that the Cu atoms in the 2D Cu boride were positively charged. In contrast, the B $1s$ spectrum showed no dependence of emission angle, and it can be fitted with a single component of the Voigt function, as shown in Fig. 4(b). The peak is naturally assigned to atoms in the 2D Cu boride layer. The binding energy of 187.8 eV determined from curve fitting confirmed that the boron atoms were negatively charged [41–43]. It is therefore likely that electrons were transferred between boron atoms and the surrounding copper atoms. The simulated XPS data generated using the 2D Cu boride model [Fig. 1(a)] indicated that all the boron sites had similar binding energies and accurately reproduced the experimental single peak, as given in the inset in Fig. 4(b). This means that all the boron atoms in the structure have similar chemical environments.

The agreement between the experimental results and theoretical simulations in this work suggests a correlation between the 1D atomic arrangement and the negative charge on the boron. This phenomenon can be explained by representing the building blocks of boron atom chains as linear molecules comprising four boron atoms terminated by two triangular boron edges. Starting with a freely optimized structure, an atomic arrangement of the molecule with two edge triangles in the *trans* configuration was derived, as depicted in Fig. 5(a). This is in contrast to the *cis* configuration [Fig. 5(b)] obtained from a 2D Cu boride model [Fig. 1(a)], in which the triangle groups lie on the surface. The discrepancy between the two structures can be resolved by considering electron doping into the molecular orbitals. In the case of the highest occupied molecular orbital (HOMO), both the *trans*- and *cis*-type 1D molecules will have the same π -type bonding. However, with regard to the lowest unoccupied molecular orbital (LUMO), the *trans*-type molecules will have σ^* -type antibonding, while the *cis*-type molecules will have π -type bonding. The addition of electrons to the LUMO causes the *trans*-type molecules to become unstable, so the *cis*-type molecules are energetically favored. Thus, the stability of 1D boron molecules can likely be attributed to these molecules having the same electronically π -type configuration as cumulenes [44,45]. The TRHEPD structural analysis assured that typical interatomic distance inside the chain is 1.6 \AA , which is much shorter than a single B-B bond in the B_2Cl_4 molecule (1.73 \AA) [46]. This observation provides support for the unsaturated bonding scheme in the boron chain. The 1D boron is therefore electronically similar to an unsaturated chain of carbon atoms, such as polycumulene [44,45]. This unique electronic configuration was previously observed in the case of boron atom chains in a bulk LiB crystal [47,48]. The 1D boron material can therefore be regarded as a cumulene-type boron that may be referred to as “bumulene.”

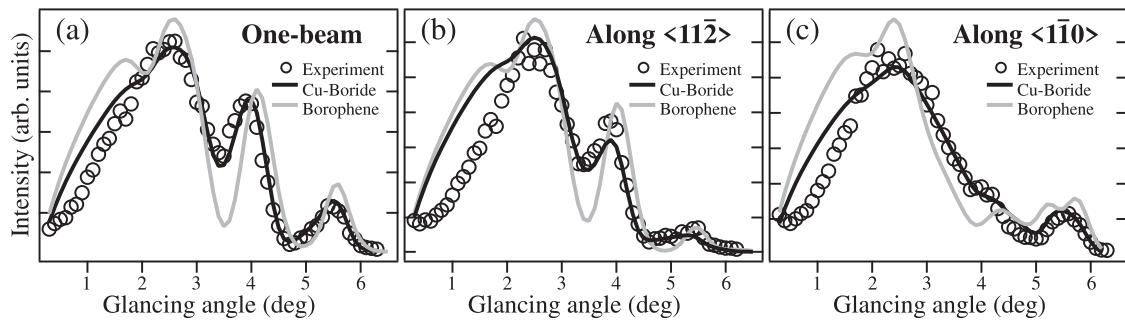


FIG. 3. Experimental TRHEPD rocking curves of Cu boride (open circles) indicating the glancing angle dependence of the beam intensity at the (00) spot taken at 10 keV. Simulated curves for the 2D Cu boride (black) and borophene (gray) models are also shown for each condition. (a) Data obtained under the one-beam condition [incident beam 10° off from the $\langle 1\bar{1}\bar{0} \rangle$ direction of the Cu(111) substrate]. Data obtained under the many-beam condition with the incident positron beam directed along the (b) $\langle 1\bar{1}\bar{2} \rangle$ and (c) $\langle 1\bar{1}\bar{0} \rangle$ axis of the Cu(111) surface. Under this condition, the simulated curve is a summation of calculated curves of the atomic models in the three domains due to the threefold rotated symmetry of the Cu(111) substrate.

As shown in Fig. 5, the molecular orbitals are expected to spread out over a greater distance than the typical B-B bond length, and the B-B interchain interaction can be non-negligible in the chain row. Figure 6(a) shows schematic drawings of the periodic array of the boron atomic chains, overlapped with the wave functions at the Γ point in the band diagram [Fig. 6(c)]. Molecular orbitals of the occupied (Γ_H) and unoccupied (Γ_L) states resemble HOMO and LUMO of the *cis*-type 1D molecules [Fig. 5(b)]. The π -type bonding can be observed in the 2D configuration of the boron chains. On the other hand, the unoccupied state (Γ_{L+1}) spatially extends between the chains. Thus, the electronic structure of the chain

rows is anisotropically 2D, as confirmed by the band diagram in Fig. 6(c). This feature is another intriguing electronic property of the boron atomic chain. Figure 6(c) also presents the 2D band structure of the Cu boride layer [Fig. 6(b)], which is consistent with those previously reported for 2D Cu borides [15]. A comparison of the two models indicates that the electronic structure of the Cu boride overlayer can be described in terms of electron filling (with an accompanying energy shift) of the boron bands and of hybridization with neighboring copper atoms. In Fig. 10 in Appendix B, band dispersion curves of a layer of the 2D Cu boride are given with the weights of the orbital compositions of copper and boron atoms. The calculation result is consistent with that from previous research [15]. One finds that compared with the band diagram of the boron chain rows shown in Fig. 6(c),

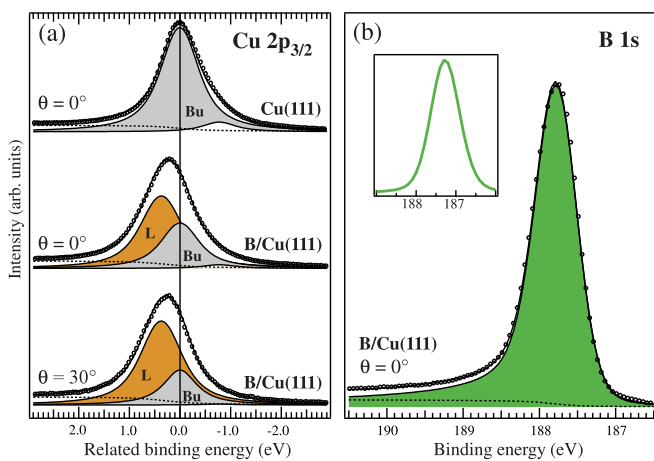


FIG. 4. XPS spectra for the boron-based material on Cu(111). (a) Cu $2p_{3/2}$ and (b) B $1s$ core-level spectra acquired at various emission angles θ with photon energies of $h\nu = 1050$ eV and $h\nu = 285$ eV, respectively. In (a), the spectrum of the clean Cu(111) surface is shown as a reference. Curve fitting of the spectra was performed using Voigt functions with a Lorentzian width of 0.7 eV based on prior work [39], together with the optimized Gaussian width. The resulting spectral components, labeled Bu and L, were found to have Gaussian widths of 0.42 eV (Bu, $\theta = 0^\circ$), 0.41 eV (L, $\theta = 0^\circ$), and 0.21 eV (L, $\theta = 30^\circ$). In (b), the B $1s$ spectrum has been curve fitted using a Voigt function with Lorentzian and Gaussian widths of 0.1 eV [40] and 0.57 eV, respectively, and the inset shows the B $1s$ spectrum, simulated with a model of 2D Cu boride on Cu(111).

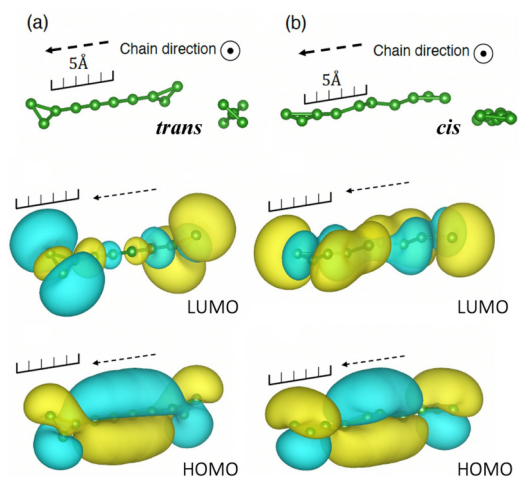


FIG. 5. Building blocks comprising the B chains along with the associated molecular orbitals. (a) A *trans*-type 1D boron molecule with triangle edges. The atomic arrangement is shown from the side and front views with the LUMO and HOMO. The LUMO and HOMO energy levels were -5.15 and -5.63 eV with reference to the vacuum level, respectively. (b) A *cis*-type 1D boron molecule with triangle edges. The atomic arrangement, LUMO (-5.32 eV), and HOMO (-5.45 eV) are shown. The color of molecular orbitals corresponds to the sign of wave functions.

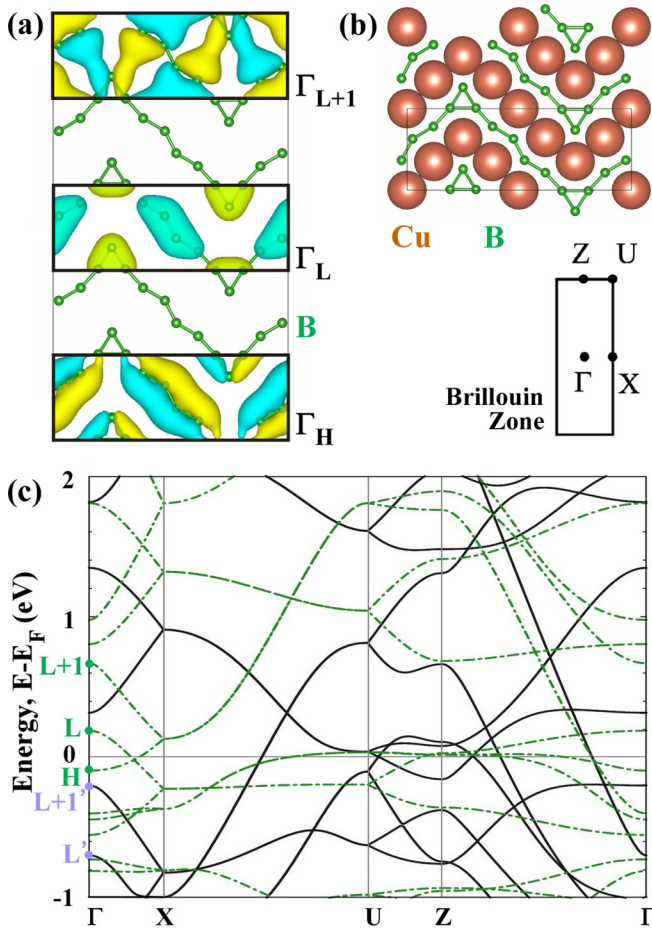


FIG. 6. Atomic chain sequences and band diagram. Structural models of (a) a periodic array of boron atom chains and (b) a freestanding Cu boride layer. A unit cell (rectangle) and the Brillouin zone are shown. (c) The band structures of the models in (a) and (b) with dispersion curves indicated in green and black, respectively. The energy is defined with respect to the Fermi level E_F . In (a), the model is schematically overlapped with molecular orbitals of states Γ_H , Γ_L , and Γ_{L+1} at Γ points that are labeled in (c). The color of the molecular orbitals corresponds to the sign of wave functions.

the electronic structure of the Cu boride overlayer can be described by electron filling (energy shift) of the boron bands and by hybridization of the boron and copper orbitals.

These microscopic features indicate that low-dimensional boron structures would be expected to exhibit unique electrophilic properties. Prior studies on 2D boron or borophene have determined that the layer itself is unstable in the freestanding form but stable on a 2D metal substrate after electron doping [16,18,49]. In the case of 2D boron, an electrical junction is achieved by sheet contact and requires a multilayer heterostructure for isolation. In contrast, electronic compensation occurs between chains of boron and metal atoms in the layer in the case of 1D boron. Therefore, a freestanding single layer would be expected to be fundamentally stable and thus could be isolated from the substrate. This could be done using an electrochemical method that was recently applied in a study involving borophene [50]. The electronic characteristics of the boron chains could be utilized to regulate the interchain

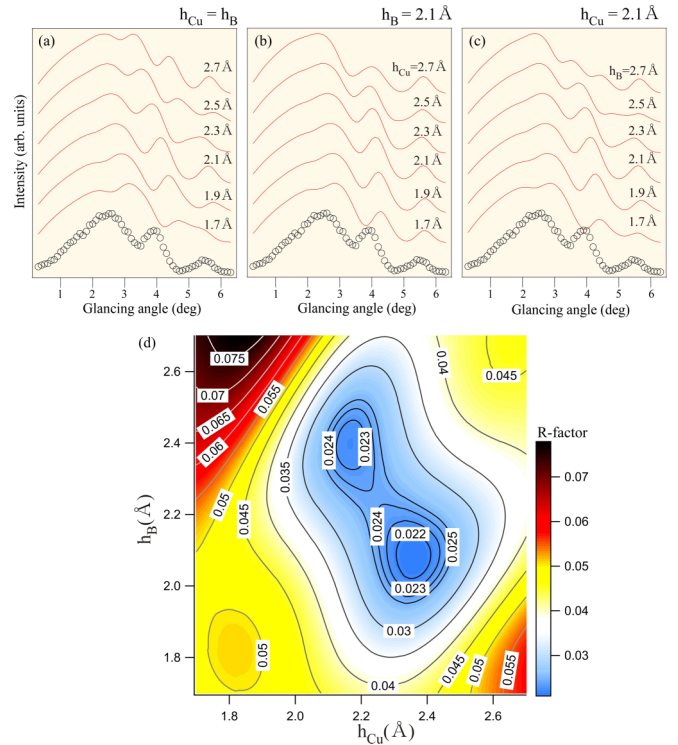


FIG. 7. The layer height dependence of the simulated rocking curve compared with the experimental result. Calculated rocking curve collection of different Cu and B chain heights with (a) $h_{Cu} = h_B$, (b) $h_B = 2.1 \text{ \AA}$ fixed, and (c) $h_{Cu} = 2.1 \text{ \AA}$ fixed. For comparison, the rocking curves from the TRHEPD experiment are shown below as circles. (d) The R -factor plot of Cu boride structures with different chain heights of B and Cu. The values of the R factors are represented by the color scale on the right.

interactions by inserting spacers, such as multiple atom wires, that make appropriate electron doping to the boron atoms. The design of such materials could allow the distances between the boron chain to be tuned and permit novel intriguing properties of this 1D system to be explored.

In reality, the bumulene-type 1D boron, at the moment, is realized as part of an alternative array of boron and copper zigzag chains in the 2D copper boride layer. Thus, future studies on the low-dimensional boron material should start with considering the 2D layer. In searching for applications of an atomic sheet, it is worth mentioning that the functionalities are generated in devices after making contacts with other materials. The present surface of the copper boride layer on Cu(111) itself can be regarded as such a model system, and thus, it is of interest to examine the influence of the substrate on the overlayer with a focus on the boron chain. We recall that the TRHEPD results in Fig. 3 favor the atomic arrangement of 2D copper boride, which is composed of a periodic array of zigzag Cu and B chains. Then, by treating the heights of the copper and boron chains as independent parameters, one can examine the structural relationships between the chains in the layer under the substrate effect. The approach is the most appropriate one for the present research since the TRHEPD measurement is sensitive enough to precisely capture changes in atomic heights at a surface. Simulations of

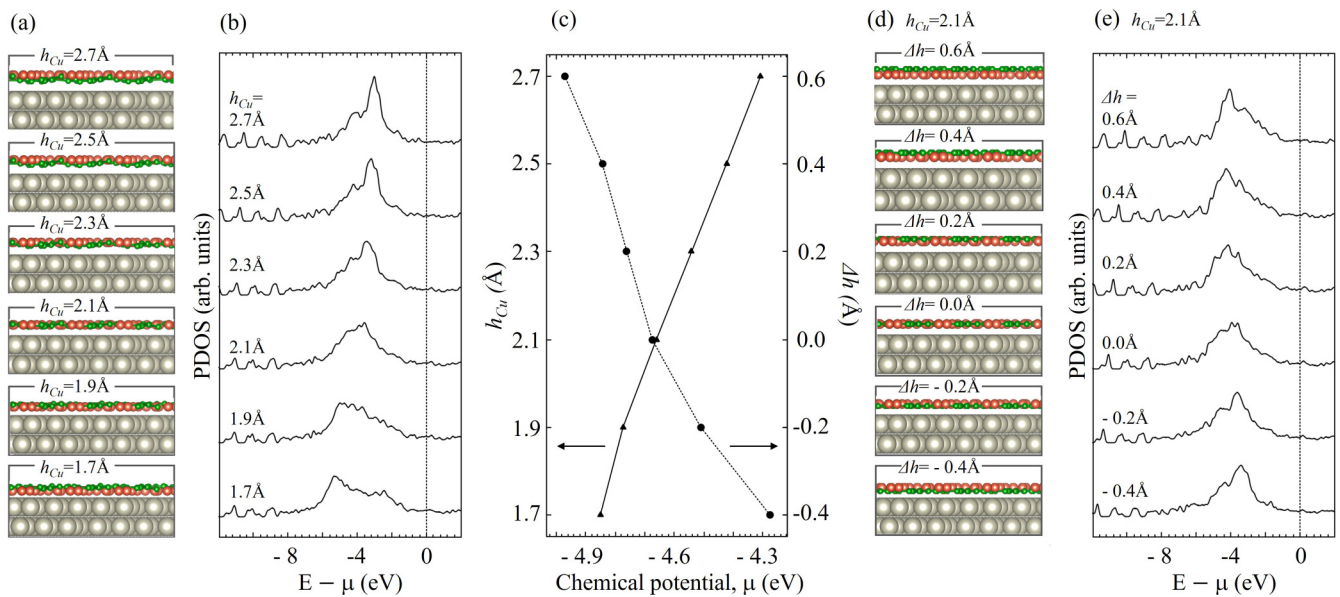


FIG. 8. Structure, layer DOS, and chemical potential of the Cu boride layers with different heights from the Cu substrate. The green, orange, and gray balls in the structures correspond to boron atoms, copper atoms in the Cu boride overlayers, and copper atoms in the Cu(111) substrate, respectively. (a) A collection of structures of Cu boride with different Cu chain heights h_{Cu} . (b) PDOS of the Cu boride overlayers in (a), where the dotted line represents the origin and corresponds to the chemical potential at each structure of different Cu chain heights. (c) Chemical potentials of the structures in (a) and (d). (d) A collection of the Cu boride structures with h_{Cu} fixed at 2.1 Å and various values for Δh . (e) PDOS of the overlayers in (d), where the dotted line represents the origin and corresponds to the chemical potential at each value of Δh .

rocking curves were carried out by keeping the same height for atoms in each chain. The heights of copper chains (h_{Cu}) and boron chains (h_B) are defined from the center position of the topmost surface layer of the Cu substrate. A collection of the simulated curves, presented in Figs. 7(a)–7(c), shows drastic differences, indicating high sensitivity to the structural parameter. To quantify the similarities between experiment and simulation, the R factor was adopted in structural analyses [19]. The factor is defined as $R = \sqrt{\sum_i [I_{exp}(\theta_i) - I_{cal}(\theta_i)]^2}$, where $I_{exp}(\theta_i)$ and $I_{cal}(\theta_i)$ are the experimental and calculated intensities, respectively, at the glancing angle θ_i in rocking curves. It is of note that structural parameters which minimize the R factor are judged the most appropriate for the atomic

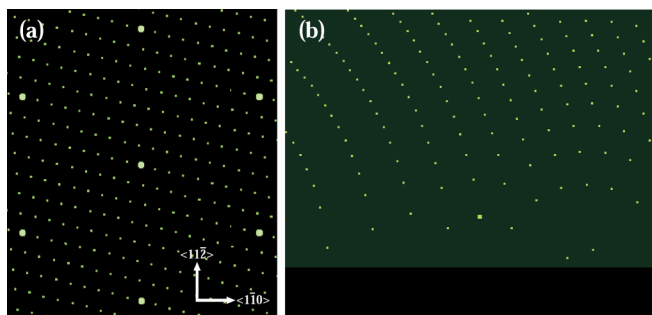


FIG. 9. Calculated electron diffraction patterns of a single domain of the $\sqrt{73} \times \sqrt{39}$ superstructure. (a) Simulated LEED pattern and (b) RHEED spot positions, respectively. The RHEED spots were simulated by an incident beam along the $\langle 1\bar{1}0 \rangle$ direction of the Cu(111) substrate.

arrangement of a sample. Figure 7(d) provides a map of the R factor with respect to the copper chain height h_{Cu} and boron chain height h_B . The absence of local minima in the R -factor map along the $h_{Cu} = h_B$ line indicates that the 2D Cu boride overlayer on Cu(111) is structurally not flat. One can

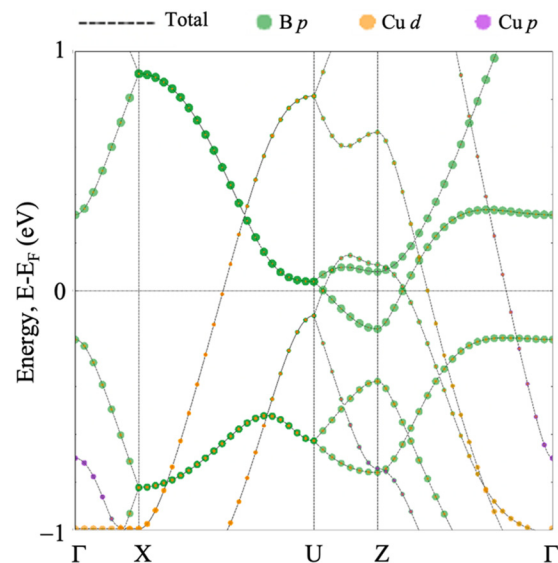


FIG. 10. Band diagram of 2D Cu boride with the weights of the orbital compositions. The contributions of individual orbitals were decomposed using the unfolding method [52]. The green, orange, and purple spheres in the diagram denote the contributions of boron p orbitals, copper d orbitals, and copper p orbitals, respectively. Their radii are proportional to the contribution of each orbital.

find the minimum around $h_{\text{Cu}} = 2.4 \text{ \AA}$ and $h_{\text{B}} = 2.1 \text{ \AA}$. The parameters are close to those reported by Yue *et al.* [15], and by changing each atom's height in the chain, the simulated curve consistently matches the model, as shown in Fig. 3. The atomic arrangement at the minimum in Fig. 7(c) was also confirmed to be stable by our first-principles calculation.

The TRHEPD analyses reveal that the copper boride layer on a metal substrate favors a structure with an atomic height modulation of $|h_{\text{B}} - h_{\text{Cu}}| = 0.3 \text{ \AA}$, which is in contrast to the flat layer in a freestanding manner expected in vacuum (Fig. 6). It was found that the atomic arrangement can be characterized by the unique parameters of the chain heights, h_{Cu} and h_{B} . Since the height corresponds to a distance between the overlayer and the crystal surface, the substrate effect can be investigated by examining the layer properties at various h_{Cu} and h_{B} values. Figure 8 demonstrates changes in the structure, electronic states, and chemical potential of the overlayer with the chain heights examined by a first-principles calculation. In Fig. 8(a), copper chains in the overlayer are fixed at various heights h_{Cu} , and heights of atoms in the boron chains are optimized. The results unveil that the boron chain atoms apparently protrude toward the substrate at $h_{\text{Cu}} > 2.1 \text{ \AA}$ but toward the vacuum at $h_{\text{Cu}} < 2.1 \text{ \AA}$. The height at $h_{\text{Cu}} = 2.1 \text{ \AA}$ can be regarded as the critical point that keeps the two-dimensionality or the flatness. For reference, the simulated TRHEPD curves of the structures in Fig. 8(a) are given in Appendix C. It is worth mentioning that one may find another local minimum around $h_{\text{Cu}} = 2.1 \text{ \AA}$, and $h_{\text{B}} = 2.4 \text{ \AA}$ in the TRHEPD results in Fig. 7(d). Optimization of boron heights in the overlayer at $h_{\text{Cu}} = 2.1 \text{ \AA}$ resulted in $h_{\text{B}} = 2.1 \text{ \AA}$ on average, indicating that structure at the local minimum is unlikely to be a part of the pristine surface.

To elucidate variations of the electronic structure of the surface system, Figure 8(b) shows a series of layer densities of states (DOSs) of the Cu boride layers in Fig. 8(a). The layer DOS is determined by a summation of the PDOS over all the orbitals in boron and copper atoms in the overlayer. One can find that the layer DOS apparently changes with h_{Cu} . The results indicate that electronic interactions exist between the layer and the substrate. The height dependence favors the hybridization scheme in the substrate effect rather than the rigid-band model for the overlayer.

Electronic evolutions of the layer structure were further examined by performing calculations based on the parameters of TRHEPD in Fig. 7. Calculations of atomic arrangements and PDOS were made by fixing the copper chain height at $h_{\text{Cu}} = 2.1 \text{ \AA}$ and by changing the height of the boron chain h_{B} without structural optimization. The height parameters are the same as the ones used in the simulated rocking curves in Fig. 7(c). To highlight modulations between the chains in the overlayer, the calculation results are given with the height difference, $\Delta h = h_{\text{B}} - h_{\text{Cu}}$. Consistent with the result in Fig. 8(b), the spectral features of the overlayer PDOS change with height, supporting the electronic hybridization picture at the interface.

A possible charge transfer between the layer and the substrate can be examined by evaluating the individual chemical potentials μ before contact. Values of chemical potentials μ are given with respect to the vacuum level based on the ESM method [32,38]. It was found that $\mu = -4.14 \text{ eV}$ for the

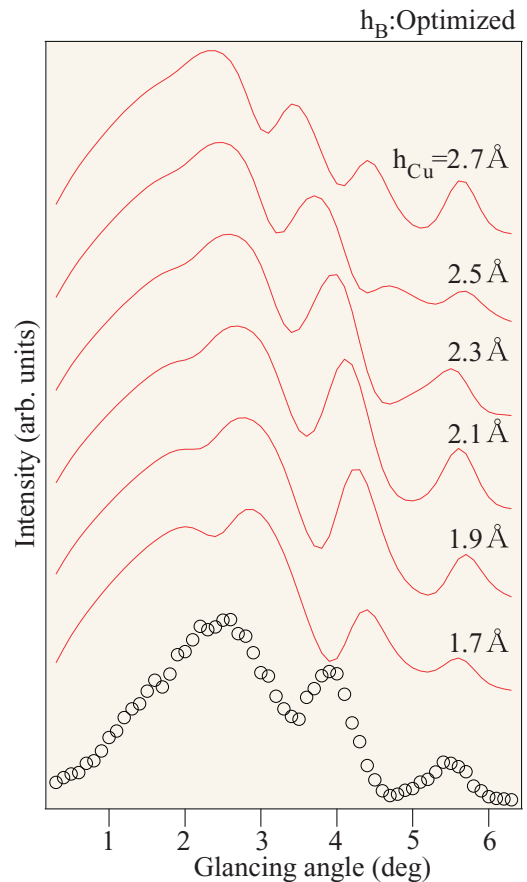


FIG. 11. Calculated rocking curves of the layer structures presented in Fig. 8(a) with the experimental result (circles at the bottom) for comparison.

pristine Cu(111) surface and $\mu = -4.96 \text{ eV}$ for the freestanding flat Cu boride layer [Fig. 6(b)]. Based on the definition, absolute values of the chemical potentials correspond to the work function. Therefore, by formation of a metal-metal contact, electronic charges flow from the substrate with the lower work function to the overlayer [51]. The calculation result indicates that the Cu boride layer is negatively charged on a metal substrate. Figure 8(c) further shows variations of μ for the interface structures of 2D copper boride on Cu(111) that are presented in Figs. 8(a) and 8(d). The value of μ becomes large or shifts to the positive side with height h_{Cu} [Fig. 8(a)] or with negative Δh [Fig. 8(d)]. The height dependence of μ is a consequence of electronic hybridization between the overlayer and the substrate, as shown in Figs. 8(b) and 8(e). In Fig. 8, one may find a tendency of the absolute value of μ or the work function to become larger when boron chains protrude toward the vacuum. Variations of the chemical potential at a contact can be modeled by the interface electric dipole, and the tendency means a relative increase in the negative charge of the dipole on the vacuum side. It is intriguing to know that this fact is consistent with the XPS results in Fig. 4 that found a negative charge of atoms in the boron chain. The calculation results in Fig. 8 demonstrate that the interface electronic structure and the interface electric dipole dramatically evolve only with the height of 1D boron in the overlayer and even with the change in a 0.2 \AA step.

With the present research, the copper boride layer on Cu(111) was found to have an alternative array of boron and copper chains that changes the relative chain height by the substrate effect. This unique feature likely indicates that electronic states of 1D boron can further be tuned by choosing an appropriate substrate. One may also be able to control the relative height between the atomic chains by changing the layer height by external fields, for example. Then, one could observe continuous evolutions of the electronic state between two and one dimensions. The copper boride layer may become a significant material for developing low-dimensional physics and for exploring new working principles in future quantum devices.

IV. SUMMARY

In summary, we investigated the structure and chemical state of a boron overlayer on Cu(111) using a combination of positron diffraction and photoelectron spectroscopy. The layer was found to comprise an ordered 2D Cu boride with a periodic array of boron atomic chains that were isoelectronic to polycumulene. First-principles calculations successfully reproduced the experimental spectrum and established that the electronic structure of this material resulted from electron doping and hybridization of the boron bands by the surrounding copper atoms. These data demonstrate that the electrophilic character of the atomic chains is unique to boron and that the alternative arrangement of boron and copper chains allows for efficient charge compensation within the layer. When the copper boride layer is on a metal surface, the relative height of boron and copper chains changes, and it is even inverted depending on the layer height or the electronic hybridization with the substrate. These properties could potentially allow the Cu boride layer to be separated from the substrate via an electrochemical treatment [50] and to be transferred on an appropriate substrate to control electronic states of 1D boron in the 2D layer.

ACKNOWLEDGMENTS

The authors are grateful to Y. Fukaya, S. Hasegawa, and J. Osterwalder for discussions. Y.T. thanks JSPS for

financial support. This work was supported by JSPS KAKENHI grants (Grants No. JP21H05012, No. JP19H04398, and No. JP18H03874), by a Grant-in-Aid for JSPS Fellows (Grant No. 21J21993), and by JST, CREST Grant No. JP-MJCR2104, Japan. This research was performed with the approval of the Photon Factory Program Advisory Committee of the Institute of Materials Structure Science (Proposal No. 2021T002) and carried out as a joint research project with the Synchrotron Radiation Research Organization and the Institute for Solid State Physics at The University of Tokyo (Proposal No. 2022A7410).

APPENDIX A: DIFFRACTION PATTERNS OF THE SINGLE-PHASE $\sqrt{73} \times \sqrt{39}$ SUPERSTRUCTURE

Figure 9 shows simulated LEED and RHEED patterns of the $\sqrt{73} \times \sqrt{39}$ phase on Cu(111) in a single-domain manner. The electron diffraction patterns in Fig. 2 can be reproduced by overlapping six different patterns of the single-phase $\sqrt{73} \times \sqrt{39}$ superstructure that were operated symmetrically using a combination of the two types of mirror reflections and three angles of threefold rotations.

APPENDIX B: BAND DIAGRAM OF THE 2D Cu BORIDE

Band dispersion curves of a layer of 2D Cu boride are given in Fig. 10 with the weights of the orbital compositions of copper and boron atoms. The calculation result is consistent with that in previous research [15]. One finds that compared with the band diagram of the boron chain rows shown in Fig. 6(c), the electronic structure of the Cu boride overlayer can be described by electron filling (energy shift) of the boron bands and by hybridization of the boron and copper orbitals.

APPENDIX C: SIMULATED TRHEPD ROCKING CURVES OF THE OPTIMIZED Cu BORIDE STRUCTURES AT VARIOUS Cu CHAIN HEIGHTS

For reference, Fig. 11 presents a collection of simulated rocking curves of the optimized structures in Fig. 8(a). The copper chain heights h_{Cu} were fixed in each structure, while heights of atoms in the boron chains are optimized.

-
- [1] *Monatomic Two-Dimensional Layers: Modern Experimental Approaches for Structure, Properties, and Industrial Use*, edited by I. Matsuda (Elsevier, Amsterdam, 2018).
 - [2] J. Ortega and F. Himpsel, in *Very High Resolution Photoelectron Spectroscopy*, edited by S. Hüfner, *Lecture Notes in Physics* Vol. 715 (Springer, Berlin, 2007).
 - [3] H. W. Yeom, S. Takeda, E. Rotenberg, I. Matsuda, K. Horikoshi, J. Schaefer, C. M. Lee, S. D. Kevan, T. Ohta, T. Nagao, and S. Hasegawa, *Phys. Rev. Lett.* **82**, 4898 (1999).
 - [4] J. R. Ahn, J. H. Byun, H. Koh, E. Rotenberg, S. D. Kevan, and H. W. Yeom, *Phys. Rev. Lett.* **93**, 106401 (2004).
 - [5] H. Morikawa, I. Matsuda, and S. Hasegawa, *Phys. Rev. B* **70**, 085412 (2004).
 - [6] E. Do, J. W. Park, O. Stetsovych, and P. Jelinek, and H. W. Yeom, *ACS Nano* **16**, 6598 (2022).
 - [7] H. Okino, R. Hobara, I. Matsuda, T. Kanagawa, S. Hasegawa, J. Okabayashi, S. Toyoda, M. Oshima, and K. Ono, *Phys. Rev. B* **70**, 113404 (2004).
 - [8] P. Gambardella, A. Dallmeyer, K. Maiti, M. C. Malagoli, W. Eberhardt, K. Kern, and C. Carbone, *Nature (London)* **416**, 301 (2002).
 - [9] *2D Boron: Boraphene, Borophene, Boronene*, edited by I. Matsuda and K. Wu (Springer, Cham, 2021).
 - [10] Z. Q. Wang, T. Y. Lu, H. Q. Wang, Y. P. Feng, and J. C. Zheng, *Front. Phys.* **14**, 33403 (2019).
 - [11] M. P. Allan, S. Berner, M. Corso, T. Greber, and J. Osterwalder, *Nanoscale Res. Lett.* **2**, 94 (2007).
 - [12] R. Wu, I. K. Drozdov, S. Eltinge, P. Zahl, S. Ismail-Beigi, I. Božović, and A. Gozar, *Nat. Nanotechnol.* **14**, 44 (2019).

- [13] A. B. Prebranjenski, A. Lyalin, T. Taketsugu, N. A. Vinogradov, and A. S. Vinogradov, *ACS Nano* **15**, 15153 (2021).
- [14] F. J. Tuli, G. Peng, S. Hossain, K. Ninomiya, R. Almed, T. Nakagawa, and S. Mizuno, *Surf. Sci.* **713**, 121906 (2021).
- [15] C. Yue, X.-J. Weng, G. Gao, A. R. Oganov, X. Dong, X. Shao, X. Wang, J. Sun, B. Xu, H.-T. Wang, X.-F. Zhou, and Y. Tian, *Fundam. Res.* **1**, 482 (2021).
- [16] B. Feng, O. Sugino, R.-Y. Liu, J. Zhang, R. Yukawa, M. Kawamura, T. Iimori, H. Kim, Y. Hasegawa, H. Li, L. Chen, K. Wu, H. Kumigashira, F. Komori, T.-C. Chiang, S. Meng, and I. Matsuda, *Phys. Rev. Lett.* **118**, 096401 (2017).
- [17] B. Feng, J. Zhang, Q. Zhong, W. Li, S. Li, H. Li, P. Cheng, S. Meng, L. Chen, and K. Wu, *Nat. Chem.* **8**, 563 (2016).
- [18] B. Feng, J. Zhang, R.-Y. Liu, T. Iimori, C. Lian, H. Li, L. Chen, K. Wu, S. Meng, F. Komori, and I. Matsuda, *Phys. Rev. B* **94**, 041408(R) (2016).
- [19] Y. Fukaya, A. Kawasuso, A. Ichimiya, and T. Hyodo, *J. Phys. D* **52**, 013002 (2019).
- [20] M. Hashimoto, Y. Fukaya, A. Kawasuso, and A. Ichimiya, *e-J. Surf. Sci. Nanotechnol.* **7**, 436 (2009).
- [21] M. Hashimoto, Y. Fukaya, A. Kawasuso, and A. Ichimiya, *Surf. Sci.* **601**, 5192 (2007).
- [22] Y. Fukaya, I. Mochizuki, M. Maekawa, K. Wada, T. Hyodo, I. Matsuda, and A. Kawasuso, *Phys. Rev. B* **88**, 205413 (2013).
- [23] Y. Fukaya, I. Matsuda, B. Feng, I. Mochizuki, T. Hyodo, and S. Shamoto, *2D Mater.* **3**, 035019 (2016).
- [24] M. Maekawa, K. Wada, Y. Fukaya, A. Kawasuso, I. Mochizuki, T. Shidara, and T. Hyodo, *Eur. Phys. J. D* **68**, 165 (2014).
- [25] A. Ichimiya, *Solid State Phenom.* **28–29**, 143 (1992).
- [26] A. Ichimiya, *Surf. Sci.* **192**, L893 (1987).
- [27] A. Ichimiya, *Surf. Sci.* **235**, 75 (1990).
- [28] T. Hanada, Y. Motoyama, K. Yoshimi, H. Iwamoto, and T. Hosi, *Comput. Phys. Commun.* **277**, 108371 (2022).
- [29] S. Yamamoto *et al.*, *J. Synchrotron Radiat.* **21**, 352 (2014).
- [30] T. Koitaya, S. Yamamoto, Y. Shiozawa, K. Takeuchi, R.-Y. Liu, K. Mukai, S. Yoshimoto, K. Akikubo, I. Matsuda, and J. Yoshinobu, *Top. Catal.* **59**, 526 (2016).
- [31] W. Kohn and L. J. Sham, *Phys. Rev.* **140**, A1133 (1965).
- [32] T. Ozaki, *Phys. Rev. B* **67**, 155108 (2003); T. Ozaki and H. Kino, *ibid.* **69**, 195113 (2004); **72**, 045121 (2005); K. Lejaeghere *et al.*, *Science* **351**, aad3000 (2016).
- [33] I. Morrison, D. M. Bylander, and L. Kleinman, *Phys. Rev. B* **47**, 6728 (1993).
- [34] J. P. Perdew, K. Burke, and M. Ernzerhof, *Phys. Rev. Lett.* **77**, 3865 (1996).
- [35] J. F. Janak, *Phys. Rev. B* **18**, 7165 (1978).
- [36] T. Ozaki and C. C. Lee, *Phys. Rev. Lett.* **118**, 026401 (2017).
- [37] C. C. Lee, J. Yoshinobu, K. Mukai, S. Yoshimoto, H. Ueda, R. Friedlein, A. Fleurence, Y. Yamada-Takamura, and T. Ozaki, *Phys. Rev. B* **95**, 115437 (2017).
- [38] M. Otani and O. Sugino, *Phys. Rev. B* **73**, 115407 (2006).
- [39] D. M. Pease, *Phys. Rev. B* **44**, 6708 (1991).
- [40] D. J. Joyner, O. Johnson, and D. M. Hercules, *J. Am. Chem. Soc.* **102**, 1910 (1980).
- [41] G. Mavel, J. Escard, P. Costa, and J. Castaing, *Surf. Sci.* **35**, 109 (1973).
- [42] C.-C. Lee, B. Feng, M. D'angelo, R. Yukawa, R.-Y. Liu, T. Kondo, H. Kumigashira, I. Matsuda, and T. Ozaki, *Phys. Rev. B* **97**, 075430 (2018).
- [43] H. Kusaka *et al.*, *J. Mater. Chem. A* **9**, 24631 (2021).
- [44] J. A. Januszewski and R. R. Tykwinski, *Chem. Soc. Rev.* **43**, 3184 (2014).
- [45] C. H. Hendon, D. Tiana, A. T. Murray, D. R. Carbery, and A. Walsh, *Chem. Sci.* **4**, 4278 (2013).
- [46] R. Köppe and H. Schnockel, *Chem. Sci.* **6**, 1199 (2015).
- [47] M. Wörle and R. Nesper, *Angew. Chem., Int. Ed.* **112**, 2439 (2000).
- [48] M. Wörle, R. Nesper, and T. K. Chatterji, *Z. Anorg. Allg. Chem.* **632**, 1737 (2006).
- [49] Z. Zhang, Y. Yang, G. Gao, and B. I. Yakobson, *Angew. Chem., Int. Ed.* **54**, 13022 (2015).
- [50] B. Radatović, V. Jadriško, S. Kamal, M. Kralj, D. Novko, N. Vujičić, and M. Petrović, *ACS Appl. Mater. Interfaces* **14**, 21727 (2022).
- [51] H. Lüth, *Surfaces and Interfaces of Solid Materials* (Springer, Berlin, 1997).
- [52] C.-C. Lee, Y. Yamada-Takamura, and T. Okazaki, *J. Phys.: Condens. Matter* **25**, 345501 (2013).